JOURNAL OF MATERIALS SCIENCE 24 (1989) 2987–2998

Influence of additions on the structure of rapidly solidified Ni_2Al_3 alloys

J. GROS, S. HAMAR-THIBAULT, J. C. JOUD
Laboratoire de Thermodynamique et Physico-chimie Métallurgiques, U.A. CNRS no. 29, ENSEEG, Domaine Universitaire, B.P. 75-38402 Saint Martin d'Hères, France

Raney nickel catalysts are prepared from Ni–Al alloys. In order to test the influence of the microstructure of the precursor alloys, we prepared homogenized and microcrystallized $(NiM)_2Al_3$ alloys with M = Cr, Cu, Fe, Ti, Zr, Ta. Microcrystallized alloys are prepared by melt-spinning. Observations were made by scanning and transmission electron microscopies. The as-melted ribbons exhibit a flower dendritic shape with NiAl as a core. An intermediate zone is observed which corresponds to small axial domains according to the peritectic formation of Ni_2Al_3 (hexagonal structure) from NiAl (b c c). Petals of the flowers are made of domains of Ni_2Al_3 almost monocrystalline. The size of the domains depends essentially on the cooling rate and on the nature of the dopant.

1. Introduction

Raney nickel catalysts are usually prepared from Ni–Al alloys. The nickel catalysts are obtained by leaching aluminium out of Al–Ni alloys by treatment with boiling sodium hydroxide solution. In the case of binary alloys Ni–Al [1] (Fig. 1), the precursor alloys contain the Ni_2Al_3, $NiAl_3$ phases [2]. The structural parameters of these phases are reported in Table I [3, 4].

Although Raney catalysts have been used industrially for a long time, the influence knowledge of the physical and chemical structure of precursor alloy upon catalytic properties is limited. The properties of the metallic catalyst may be modified by some metallic associations. Cr-, Fe-, Mo- and Cu-doped variants are often used [5, 6]. Chromium has received particular attention as dopant for enhancing the activity and the selectivity of some reactions. The changes in catalytic properties can be ascribed to a change in electronic factors of the active sites and to restructuring of the metal atom arrangement at the surface [7].

The aim here is to correlate the catalytic performance with different parameters at the precursor alloy level. Essentially, two different treatments have been performed in order to obtain various and well-characterized metallurgical $(NiM)_2Al_3$ structures. Homogenization annealings at high temperature have been performed to obtain large single Ni_2Al_3 phase. Rapidly quenching from high temperature is used in order to obtain large amounts of dopants randomly distributed in the present phases and also a supersaturation of dopant in the phases. The composition and structure of the alloy is checked by metallurgical characterizations. Attention has been paid to the chromium-doped alloys. The metallurgical structures were compared with those of other doped $(NiM)_2Al_3$ alloys (M = Fe, Cu, Ti, . . .).

So, from the starting alloy, the composition of which is based on $Ni_{40}Al_{60}$, three precursor alloys are obtained, heterogeneous, homogenized and microcrystallized. After a comparative study of these three precursor alloys, the catalysts prepared from the precursors will be tested. The manner in which these catalysts are generated, which is a very important factor for industrial applications, must be checked in order to be able to have complete control over the texture of the catalyst.

2. Experimental procedure

2.1. Alloy preparation

The composition of investigated alloys is of $Ni_{2-x}M_xAl_3$ type, with M = Cr, Fe, Cu or Ti. To enable comparison, x is kept equal to 2 at %. It must be noticed that only a few ternary phases diagrams are known in this composition range [8–10].

The starting alloys were prepared by co-fusion of the elements by IMPHY SA. First, annealings were performed at different temperatures below the peritectic point at 1133° C in the Ni–Al system (Fig. 1) and for different times (from 2 days to 1 month) in order to obtain the thermodynamical equilibrium. The number of phases depends on the nature of the dopant as seen later.

The second method used to prepare another type of structure is melt-spinning, which gives rise to microcrystallized alloys [11, 12]. This elaboration technique consists in induction melting in a crucible, which has a nozzle (diameter 0.8 mm) through which the molten metal is ejected onto a copper-cooled surface. The castings are performed under helium atmosphere. The temperature of the liquid metal before ejection is kept at about 1560° C. The extruded molten metal in contact with the casting surface solidified as a ribbon. The influence of the ejection pressure and the rolling velocity (diameter of the casting surface = 300 mm) on the microstructure of the alloys has been studied [13].

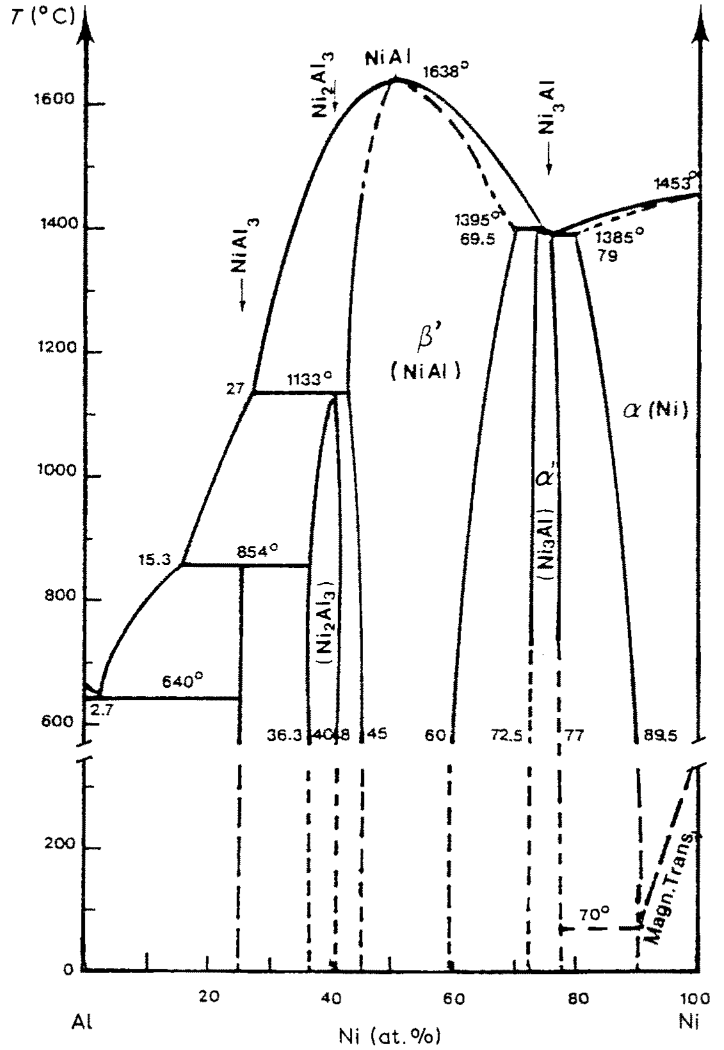

Figure 1 Binary diagram Ni–Al from [1].

2.2. Investigation methods

Sample surface observations are examined by scanning electron microscopy (SEM-JSM.35) fitted with an energy dispersive X-ray analysis system (Tracor-NS80). Phase composition in as-cast and annealed alloys is determined by quantitative calculations based on a ZAF program [14]. Cross-sections of microcrystallized alloys are also observed. X-ray analyses are performed on all samples but it must be noticed that the X-ray lines of NiAl are superposed with those of Ni_2Al_3.

More accurate observations are carried out by transmission electron microscopy (TEM-JEM.200CX) on foils electrolytically thinned in an acid solution (perchloric acid 10%, acetic acid 90%) at room temperature. EDS analyses are obtained with a VG-HB5-STEM, with a resolution of 1.5 nm at the sample level.

2.3. Preparation of an Ni–Raney catalyst

Raney catalysts are usually prepared by removing aluminium from the Ni–Al phase, by an alkaline solution. The relationship between the microstructure and the texture of the catalyst prepared from these alloys, with thin foils of well-characterized $(NiM)_2Al_3$ microcrystallized precursors was studied by TEM. The alloys are converted into nickel by treatment with boiling NaOH6N solution.

3. Experimental results

3.1. As-cast and annealed alloys

All the as-cast 2 at % doped alloys are multiphased. Typical SEM images of Cr, Fe, and Ti as-cast alloys are shown in Fig. 2. With copper as doping agent, the as-cast alloy presents only one phase with traces of a second phase. In the case of Cr-, Fe-doped alloys, two phases are distinguished. Their compositions are reported in Table II. The composition of the major part of the sample is the M-poor phase with partial substitution of Ni by M to give the stoichiometry such as $(NiM)_2Al_3$. Grains of this phase are surrounded by a thin layer of a darker M-rich phase whose compositions are respectively $NiCr_3Al_9$ and $NiFeAl_7$ in the case of Cr or Fe dopants. The $NiCr_3Al_9$ phase may be compared to the well-known phase Cr_4Al_9 reported in

TABLE I Crystallographic structure of the different phases occurring in the binary system Ni–Al [3, 4]

Compound	Space group		Lattice parameter (nm)		
			a	*b*	*c*
Al	Fm3m	Al	0.4049		
Al_3Ni	Pbnm	Do_{11}	0.4812	0.6661	0.7366
Al_3Ni_2	P3ml	$D5_{13}$	0.4036		0.490
AlNi	Pm3m	B2	0.2886		
Ni_3Al	Pm3m	$L1_2$	0.3561		
Ni	Fm3m	Al	0.352		

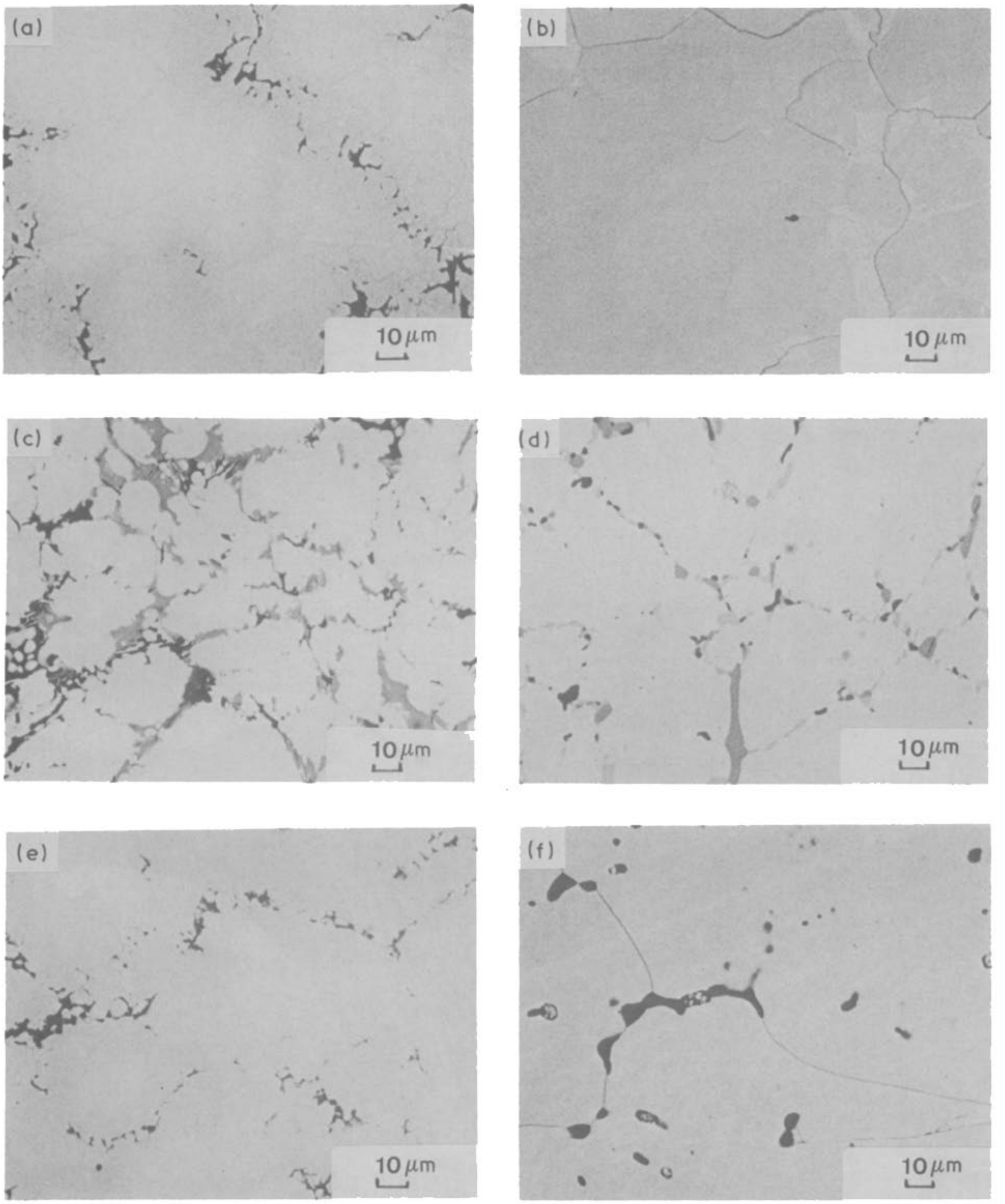

Figure 2 SEM images of (a, b) Fe-, (c, d) Ti- and (e, f) Cr- as-cast and annealed alloys. (a, c, e) As-cast, (b, d, f) annealed.

Al–Cr binary diagram. The ternary phase diagram Ni–Cr–Al is not known over all the concentration field and particularly in our composition range. Calculated section [8] shows a very small domain of homogeneity for the Ni_2Al_3 phase (Fig. 1). For the Fe-doped alloy, the ternary phase diagram has been described by Khaidar [10] at 1000° C, the Ni_2Al_3 phase can dissolve up to 10 at % of Fe (Fig. 3a) and the Fe-rich phase may be compared with the ternary $NiFeAl_9$ phase. The Ti-doped as-cast alloys present three phases. The first one has the composition of Ni_2Al_3. The second contains 20 at % Ni and 10 at % Ti and is compared to the $NiTiAl_2$ phase. The third phase has the composition $NiAl_{6.5}Ti_{2.5}$. These observations are in good agreement with the work of Nash *et al.* [9] who show a calculated section at 800° C with a very small domain of homogeneity of the Ni_2Al_3 phase (Fig. 3b).

As shown in Fig. 1, the Ni_2Al_3 phase is formed peritectically at 1133° C from the NiAl phase

$$NiAl + liq \rightleftharpoons Ni_2Al_3$$

The doped-alloys are heated at a lower temperature, indicating that the temperature of the peritectic reaction falls significantly with 2 at % addition with Fe or Cu as dopant. The temperature is held for a time long enough to allow coarsening of the structure and to obtain equilibrium between the phases.

After 2 and 17 days at 1000° C, respectively, Cu-

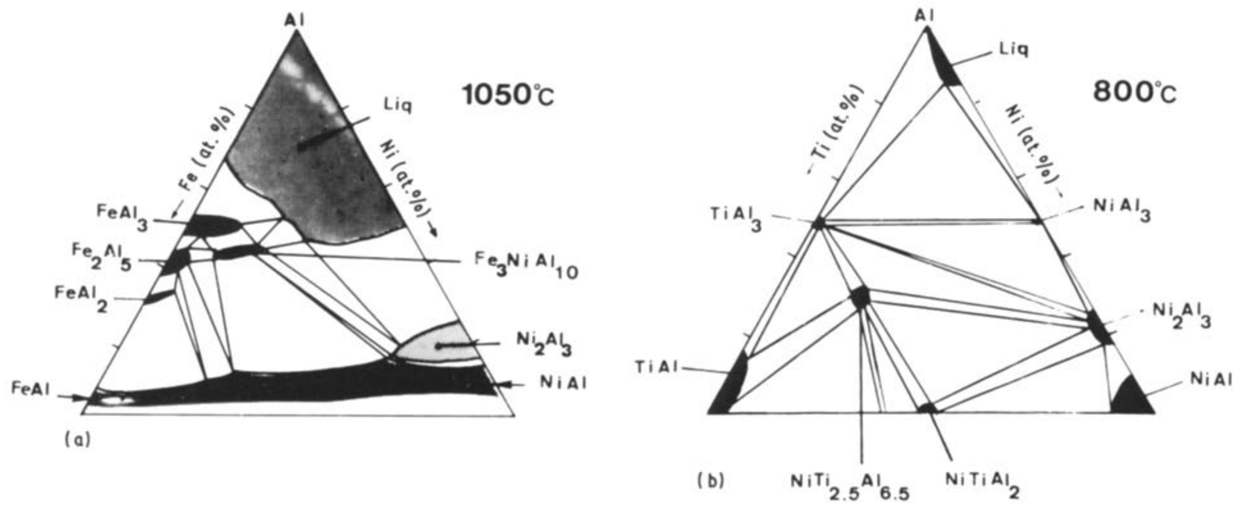

Figure 3 Ternary systems Al–Ni–M. (a) M = Fe from [10], and (b) M = Ti from [9].

and Fe-doped alloys are monophasic. Heating at this temperature gives rise in the case of Cr and Ti alloys to a liquid. In the case of Cr alloy, structures after annealing at 950° C, during 7 to 26 days, show large grains (about 200 μm diameter) with a composition of $(NiCr)_2Al_3$ as reported in Table II. Particles of a second phase (as previously shown in the as-cast alloy) are observed all around the grains even after 26 days. Although a precise evaluation was not performed, the SEM images suggest that the amounts of Cr-rich phase are less than 5 vol % for the as-cast alloy and 1 vol % for the annealed one. The Ni level is lowered from 8 to 5 at % after 17 days; then the composition of this phase remains constant and gives rise to the composition $(NiCr)_5Al_8$. After 18 days at 950° C, the Ti-doped alloy shows a stable state, representing the equilibrium structure between the phases Ni_2Al_3, $NiTiAl_2$ and $NiAl_{6.5}Ti_{2.5}$ (Table II and Fig. 3b), according to Nash *et al.* [9].

3.2. Microcrystallized alloys

Our aim, using a melt-spinning method, is to make a microcrystallized structure with a regular and homogeneous grain-size distribution. Continuous ribbons cannot be made with our type of alloy. Very small and brittle pieces (10 mm long) are obtained.

3.2.1. Cross-section of a ribbon

According to the literature [15–18], the highest cooling rate and the largest undercooling is expected on the wheel side, where the crystallization starts with heterogeneous nucleation. On this side, a very fine-grained zone (I) is expected. As shown in Fig. 4a, such a zone is not detected in Cr-doped alloys due to the smaller size ($< 0.1\ \mu$m). The typical microstructure of a Cr-microcrystallized alloy clearly exhibits only two distinct regions: a columnar dendritic zone (II), and an equiaxed dendritic zone (III). Some nucleii of zone I succeed in growing into the ribbon as columnar

TABLE II Composition of the different phases in the as-cast (as) and annealed alloys (number of days and temperature).

Alloy			Composition (at %)			Phases
			Ni	X	Al	
	Ni_2Al_3	Matrix	41.151		58.85	Ni_2Al_3
Cu						
	as	Dark phase	39.4	*	60.6	Ni_2Al_3
		Hell phase	25.9	*	74.	$NiAl_3$
	2d 1000° C	Homogeneous	41.5	*	58.5	Ni_2Al_3
Cr						
	as	Hell phase	40.4	0.8	58.8	$(NiCr)_2Al_3$
		Dark phase	7.8	26.1	66.1	$Al_9(CrNi)_4$
	17d 950° C	Hell phase	39.6	1.9	58.5	$(NiCr)_2Al_3$
		Dark phase	4.7	33.8	61.5	$Al_8(CrNi)_5$
Fe						
	as	Hell phase	38.9	2.0	58.9	$(NiFe)_2Al_3$
		Dark phase	14.3	13.1	72.6	$(NiFe)Al_9$
	12d 1000° C	Homogeneous	37.2	2.7	60.1	Ni_2Al_3
Ti						
	as	Hell phase	41.3		58.7	Ni_2Al_3
		Dark phase	24.0	12.4	63.6	$(NiTi)_2Al_3$
		Darker phase	8.2	20.6	71.0	$NiAl_{6.5}Ti_{2.5}$
	18d 950° C	Hell phase	40.4	0.3	59.3	Ni_2Al_3
		Dark phase	22.7	16.2	61.1	$NiTiAl_2$
		Darker phase	10.5	18.5	71.0	$NiAl_{6.5}Ti_{2.5}$

*Analysis is not possible (superposition of X-rays) crystals (II). An inclination of the columnar crystals of about 20° is observed and may be explained by a deviation of the highest thermal gradient from the ribbon normal or by a flow at the crystallization front [15].

Above the columnar dendritic zone, there is a branched equiaxial dendritic zone (III). With increasing rolling velocity, a small increase in width of the columnar zone was observed although it does not exceed 10% of the thickness of the ribbon. The size of the equiaxed dendrites remains almost the same through the cross section of the ribbon, but is a function of rolling velocity. The diameter of the grains decreases from 6 to 2 μm when the rolling velocity increases from 22 to 39 m sec^{-1}. The ejection pressure has no effect on the microstructure of the ribbon. The equiaxed dendrites have been called daisies.

SEM observations of all the various castings indicate that the ribbon with the casting parameters of $P = 250$ mbar and $V = 39$ m sec^{-1} (2500 r.p.m.) presents regular-shaped ribbon pieces and homogeneous grain distribution. The thickness is approximately 75 μm, its width is 1 mm. The size of the grains is 5 μm. SEM analyses show that the Cr-doped crystallized alloys have the same nominal composition as the starting alloys. Moreover, there is no Cr-segregation in the thickness of the ribbon and the composition is the same in the two zones (equiaxial and columnar).

The Cu- and Fe-doped microcrystallized ribbons are comparable with the Cr-doped one with only two detectable zones (II and III). In Ti-doped microcrystallized ribbon, at the wheel contact side a very small equiaxed zone (I) is observed as shown in Figs 4b, c and its width is estimated between 0.5 and 1 μm.

3.2.2. Morphological characterization of the castings (Cr additions)

In the case of the Cr-doped alloy, several castings were made with different values of ejection pressure P (mbar), and rolling velocity, V (m sec^{-1}). The ejection pressure P (from 200 to 400 mbar), has no significant effect on the width of the ribbon. As shown in Fig. 5, the rolling velocity affects the thickness of the ribbon. For a constant pressure of 200 mbar, the thickness decreases from 100 to 40 μm when the rolling velocity increases from 22 m sec^{-1} (1400 r.p.m.) to 47 m sec^{-1} (3000 r.p.m.).

An attempt is made to correlate the decrease in thickness, e, with the increase in rolling velocity, V. Hillman and Hilzinger [19] assumed that during cooling, when the molten metal is in contact with the casting surface, the bulb formed by this metal is a semi-infinite space. They obtained a relation of the following type:

$$e = kV^{-p}$$

where p depends on the nature of the thermal transfer during cooling. p is, respectively, equal to 0.75 and 1.5 for a perfect or a Newtonian cooling. We found experimentally $p = 1.38$, which corresponds to a Newtonian thermal transfer.

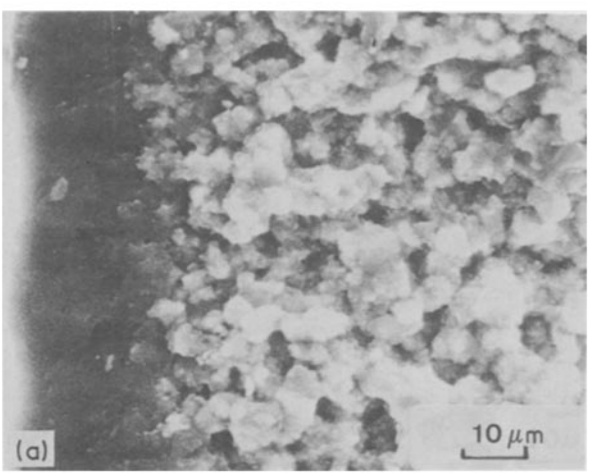

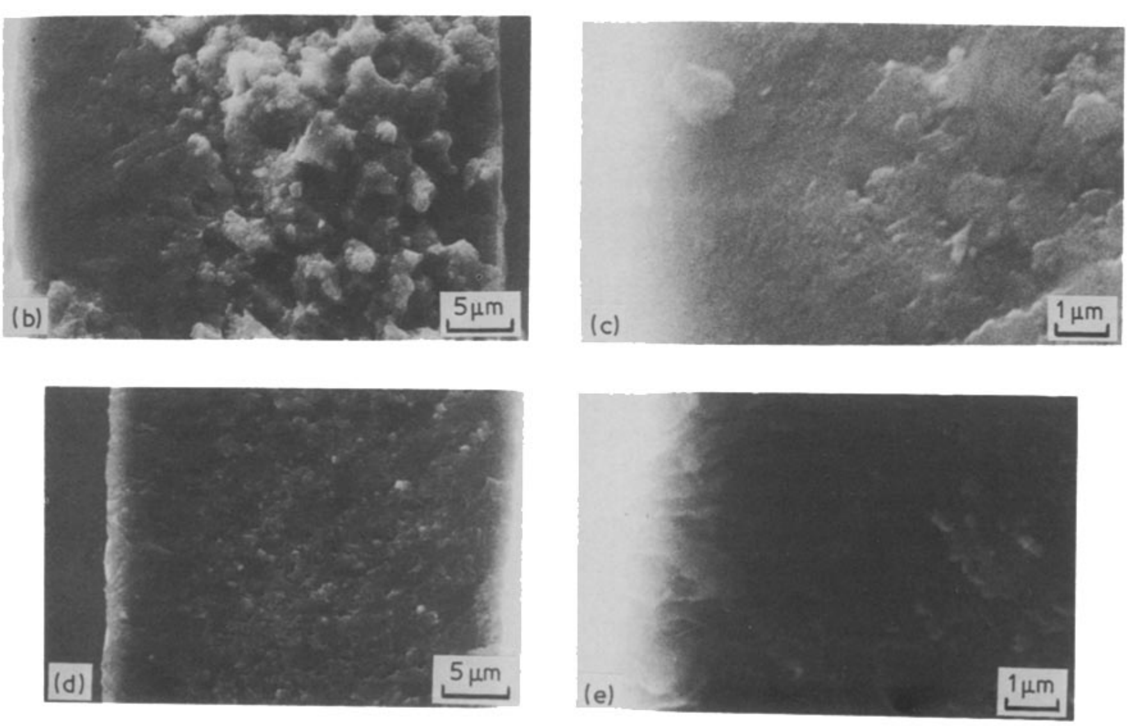

Figure 4 Cross-sections of (a) Cr-, (b, c) Ti- and (d, e) Ta-doped microcrystallized alloys, showing two or three zones.

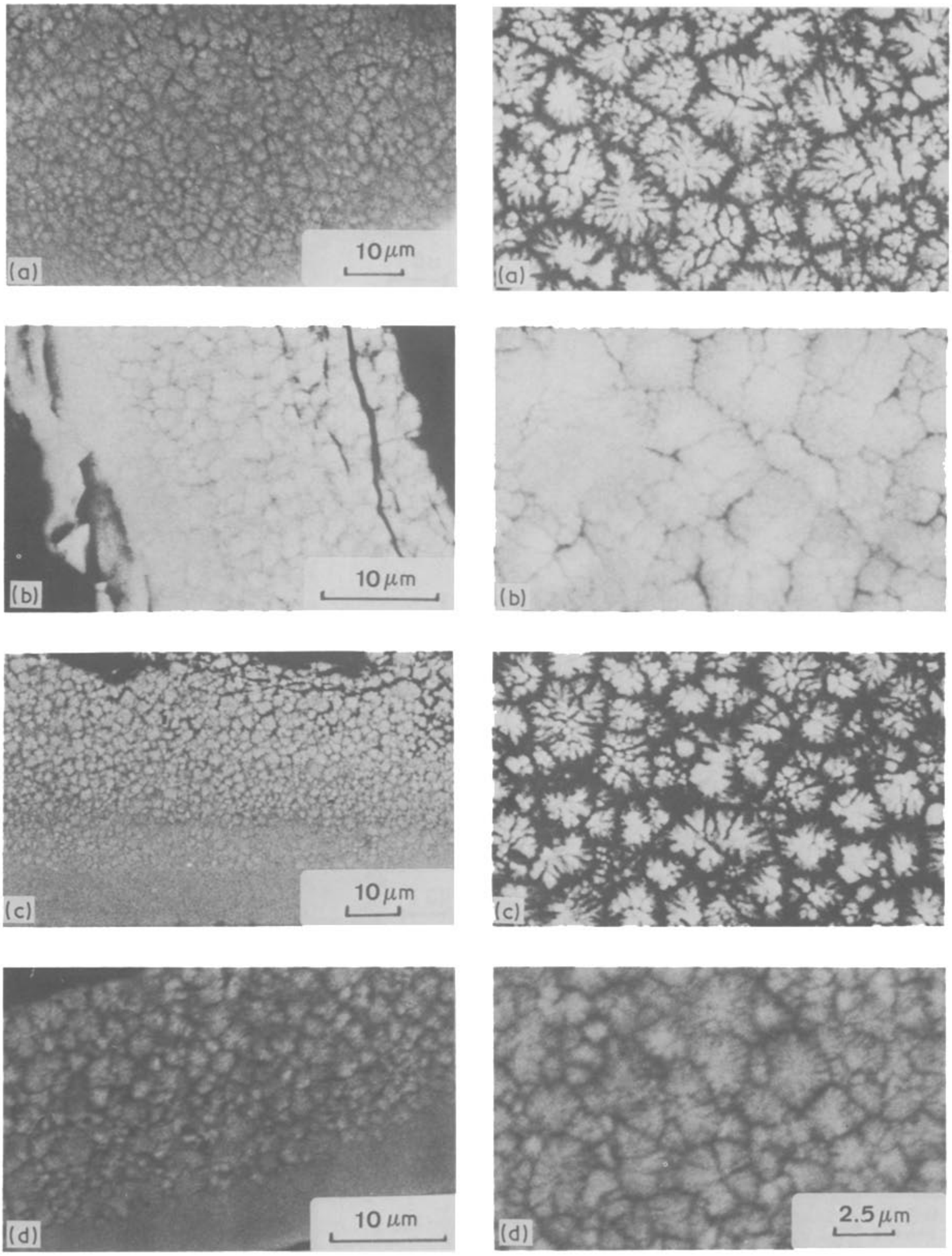

Figure 5 Variations of thickness of the ribbons with rolling velocity. P = 200 mbar, V = (a) 22, (b) 28, (c) 31, and (d) 34 m sec^{-1}.

3.2.3. Characterization of a dendritic grain

First, we present some observations in the case of Cr-doped alloys, then comparison with other dopants will be made.

As shown in the SEM images (Fig. 6), the grains appear with a daisy dendritic shape. In all Cr-castings made with a low wheel velocity (< 30 m sec^{-1}) the daisy shape is well defined. As previously mentioned, the mean diameter of the grains decreases from 6 to 2 μm, when the rolling velocity of the wheel increases from 22 to 39 m sec^{-1}.

TEM observations show that the grains present a very complex structure as shown on the schematic representation (Fig. 7). The foil plane is parallel to the ribbon surface. Four different parts (C, I, H, E) may be observed. The size of these four parts depends on different parameters: the cooling rate for a dopant; the nature of the dopant.

3.2.3.1. Influence of cooling rate in the case of Cr-doped alloys. For slow cooling rate (< 30 m sec^{-1}), the shape of the grains is almost independent of the casting

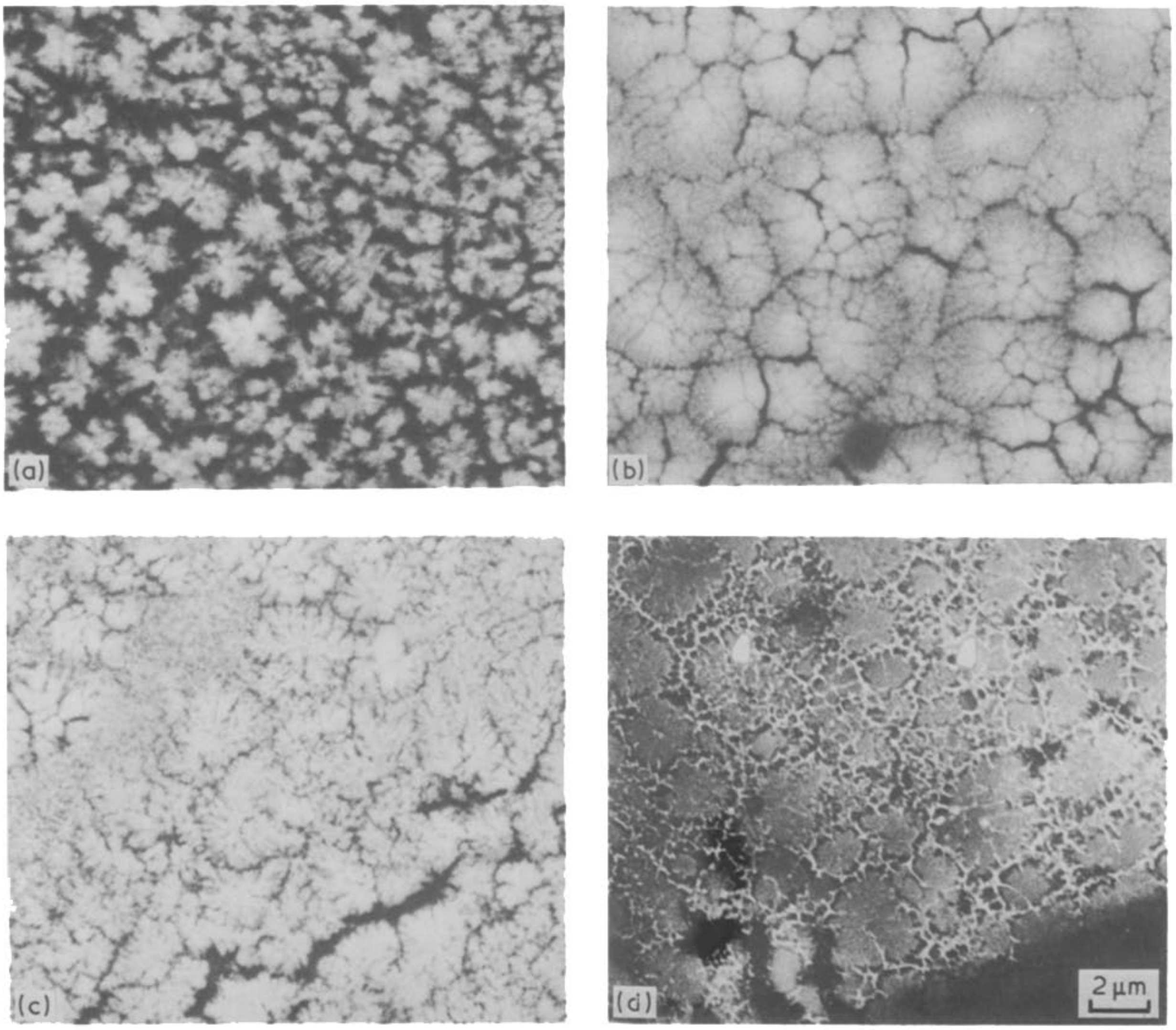

Figure 6 SEM observations of dendritic grains for (a) undoped and with (b) Cr-, (c) Ti- and (d) Ta-dopants.

parameters. The central part (C) of the daisy (Fig. 8a) is constituted by the well-crystallized body-cubic centred NiAl phase (Table I). This core exhibits square or hexagonal dislocation networks which are comparable to that observed in the high-temperature deformed NiAl phase by some authors [20]. These dislocations are attributed to thermal stresses occurring during quenching. The mean diameter of this core is almost 0.5 to 1 μm for a wheel velocity of $V = 28\,\mathrm{m\,sec^{-1}}$. Related to the surface of the ribbon, the orientation of the NiAl core is near the $\langle 1\,0\,0\rangle$ direction. The $\langle 2\,1\,0\rangle$ and $\langle 3\,1\,1\rangle$ directions are often detected. These $\langle 2\,1\,0\rangle$ and $\langle 3\,1\,1\rangle$ directions formed angles of 26.56° and 25.23°, respectively, which represent deviations from the $\langle 1\,0\,0\rangle$ direction. An NiAl core with orientations such as $\langle 1\,1\,0\rangle$ or $\langle 1\,1\,1\rangle$ with respect to the surface of the ribbon was never detected. This deviation of 25° from the $\langle 1\,0\,0\rangle$ direction is directly related to the inclination of the columnar crystals.

As shown in Fig. 8b, the petals of the daisy for the slow cooling rate are large domains of hexagonal Ni_2Al_3 phase. Almost all these large monocrystalline Ni_2Al_3 domains show concentrations near the $\langle 0\,0\,0\,1\rangle$ and $\langle 1\,1\,\bar{2}\,1\rangle$ directions. Between the well-defined daisies, small crystals (E) without any orientation relationship, are observed where the NiAl, Ni_2Al_3 and $NiAl_3$ phases may be indexed. In this external part,

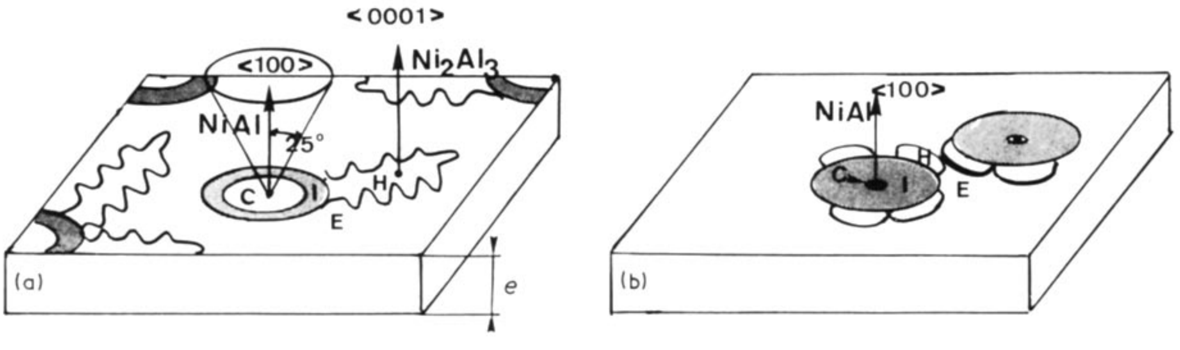

Figure 7 Schematic representation of the structure of grains for two rolling velocities: (a) 28 and (b) $39\,\mathrm{m\,sec^{-1}}$.

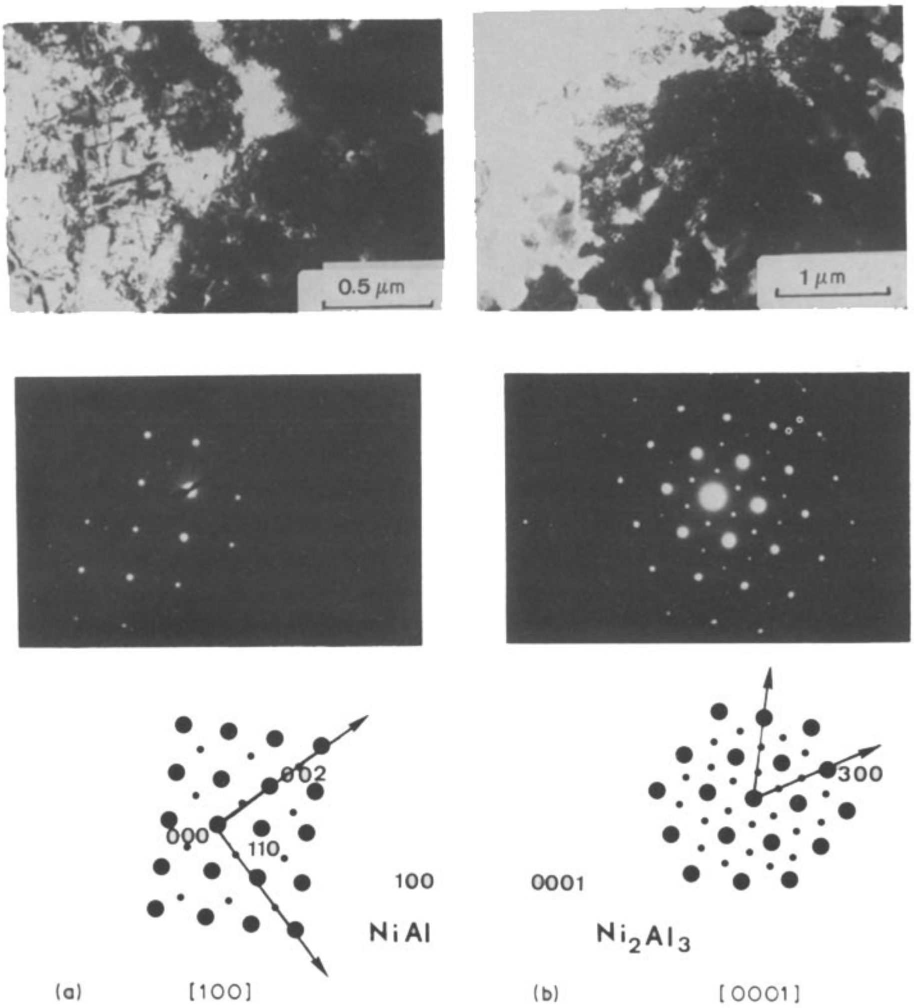

Figure 8 TEM observations and diffraction patterns of Cr-microcrystallized alloy showing the complex structure of the dendritic grain ($V = 28\,\mathrm{m\,sec^{-1}}$). Centre of the grain = NiAl (a) and petals of Ni_2Al_3 (b).

some chromium segregations were found, but no Cr-rich phases (such as Al_8Cr_5 or Al_9Cr_4) were observed as in as-cast and annealed Cr-alloys (Fig. 9a).

Between the NiAl core (C) and the Ni_2Al_3 petals (H) of the daisy, a narrow field (I) was detected showing a very complex diffraction pattern (Fig. 10a). These diffraction patterns are indexed as a superposition of ordered domains of Ni_2Al_3 (axial domains), whose orientations are directly related to the NiAl cell.

After annealing at 350° C, no significant change in this complex microstructure is observed. However, growth of the small axial domains of Ni_2Al_3 in the intermediate zone (I) was noted.

For higher cooling rates ($V > 35\,\mathrm{m\,sec^{-1}}$), the shape of the grains changes. It becomes more spherical and the mean diameter decreases. It is about $2\,\mu\mathrm{m}$ for $V = 39\,\mathrm{m\,sec^{-1}}$. The NiAl core (C) and Ni_2Al_3 petals (H) also become smaller. But the intermediate zone (I) increases, becomes very large and almost all the grain is formed with this zone (Fig. 7b). The change in grain morphology from daisy dendritic to spherical seems to occur abruptly for a wheel velocity of around $35\,\mathrm{m\,sec^{-1}}$ as shown in Fig. 11.

3.2.3.2. Influence of the nature of the dopant. Microcrystallized ribbons of Cu- Fe- or Ti-doped or undoped alloys also exhibit the same dendritic structure. The grains show the same complex structure with four zones, but the respective size of these different regions depends on the nature of the addition. With Cu-, Fe-as dopants, the size of the daisy is almost the same as in Cr-doped microcrystallized alloys, but the NiAl core (C) is smaller ($< 0.5\,\mu\mathrm{m}$), and the intermediate zone (I) seems larger ($0.5\,\mu\mathrm{m}$). No segregation of Cu or Fe is observed in the daisies.

The Ti-doped microcrystallized grains are larger. The size is approximately $6\,\mu\mathrm{m}$. The daisies are formed of large monocrystalline Ni_2Al_3 domains (Fig. 6c). The NiAl core and the intermediate zone are very small, and the size of these two zones remains smaller than $0.5\,\mu\mathrm{m}$. Between the daisies (E) little bridges are observed formed with a Ti-rich phase (Fig. 9b) of composition $NiTiAl_2$ in good agreement with the Al–Ni–Ti ternary diagram (Fig. 3b) [9].

3.3. Observation of short-range order

Some electron diffraction patterns of as-quenched alloys exhibit diffuse intensities between the reciprocal lattice points. The diffuse intensity may be attributed to short-range order (SRO) of the vacancies in the Ni sublattice, giving rise to the formation of the superlattice Ni_2Al_3 from the primitive NiAl cell. De Ridder *et al.* [21] show effectively that a transition state may occur near the stoichiometry $Ni_{0.66}\square_{0.33}Al$. This transition state is characterized by a seven-point cluster of the Ni-sublattice composed of an Ni site and its six

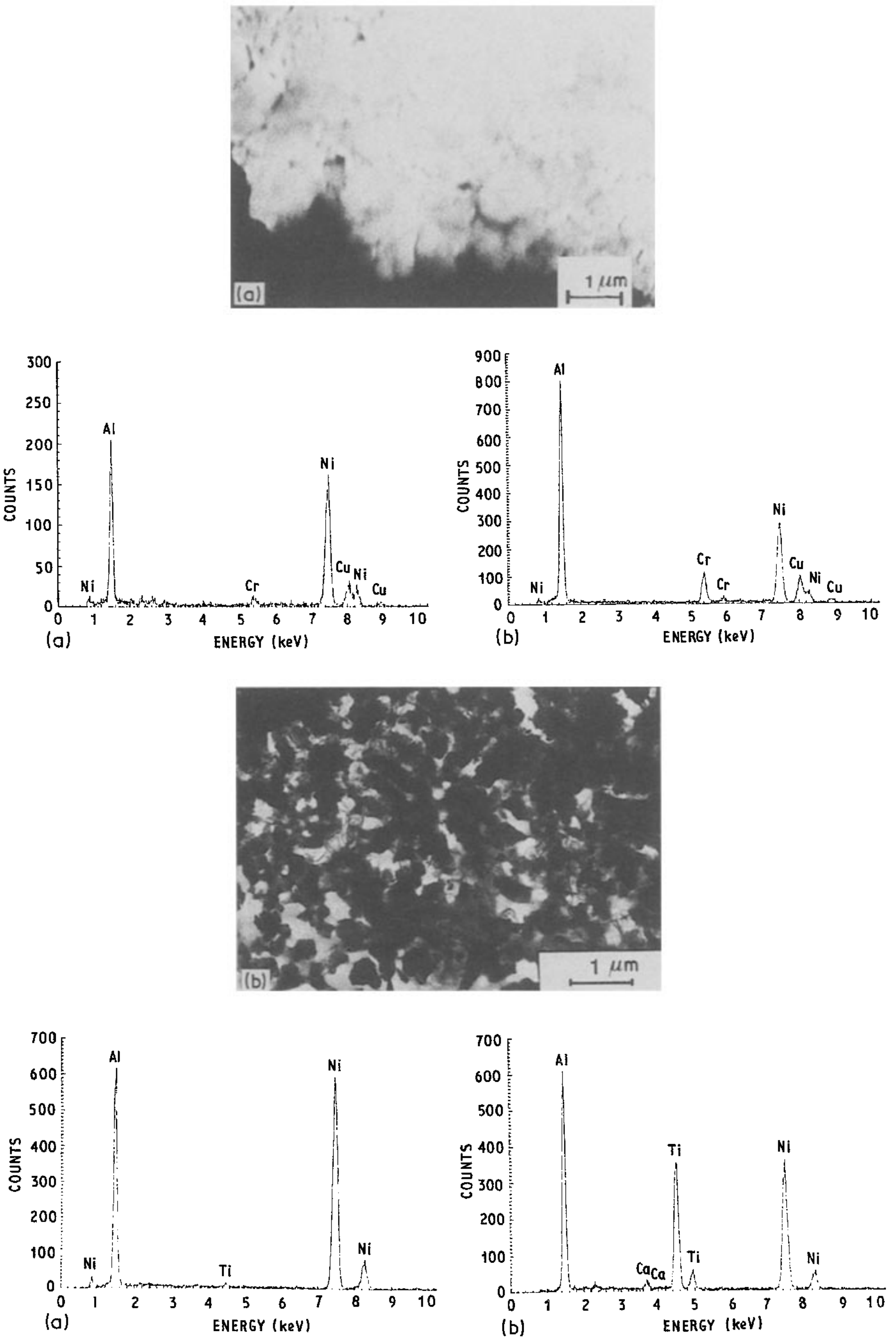

Figure 9 STEM-EDS analysis showing the microsegregation in the (a) Cr- and (b) Ti-microcrystallized alloys.

nearest neighbours. This ordering may be considered as a prefiguration of the long-range ordered structure Ni_2Al_3. It is difficult to investigate diffuse scattering regions because of their small extension. However, they have been located between the NiAl core and the axial domains of Ni_2Al_3 of the intermediate zone (I). The extension of this transition state depends on the dopant and is directly related to the size of the intermediate zone. With Cr addition the intermediate zone is very small and no diffuse scattering regions are observable. With Cu and Fe additions, the behaviour of the alloys is similar to the undoped alloy, diffuse intensity is observable and the transition zone is detectable.

3.4. Orientation relationship between Ni crystallites and Ni_2Al_3 alloys

Treatment with hot NaOH solution for up to 1 h, has been performed on microcrystallized alloys in order to examine the evolution from precursor alloy to the catalyst sponge during Al-leaching.

The different parts of the precursor microcrystallized alloys are attacked selectively. In the case of Cr-doped alloy, the external zone is rapidly attacked. The large domains of the Ni_2Al_3 phase disappeared. The NiAl core (C) remains unattacked and exhibits diffraction patterns which are characteristic of the b c c NiAl phase.

The intermediate NiAl crystallites exhibit a typical orientation relationship with the primitive Ni_2Al_3 phase. We observed unambiguously an hexagonal ordered phase Ni_2Al of the same space group as Ni_2Al_3, which is not mentioned in the binary phase diagram, but is comparable with the Ni_2Al phase described by Reynaud [22]. Around the NiAl core, we observed small fields of unattacked Ni_2Al_3 and Ni crystallites. These Ni crystallites are similar to the

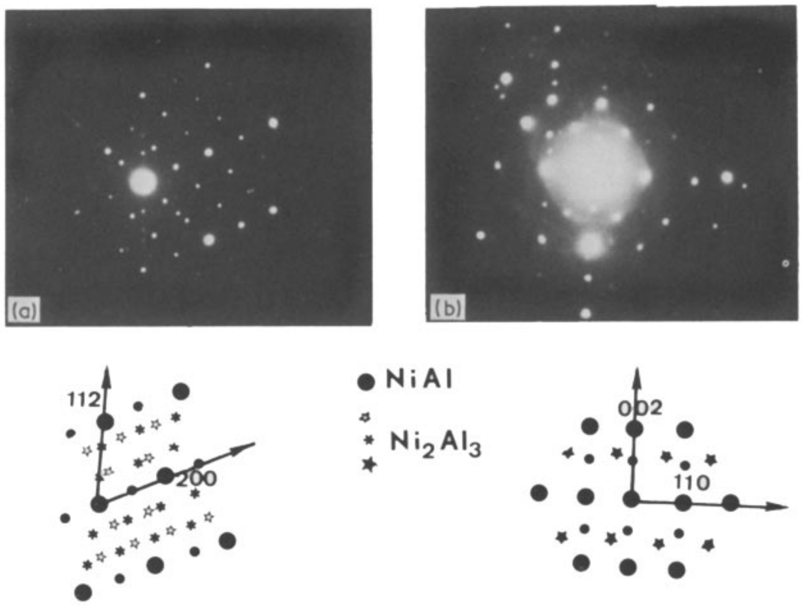

Figure 10 Diffraction patterns in the intermediate zone (a) showing the Ni_2Al_3 axial domains and in the external part of the daisy (b).

sponge observed by Delannay [23] and Birkenstock *et al.* [24].

The Ni fcc crystallites can be deduced from the NiAl structure using a Bain transformation. This transformation is well known as nondiffusive transformation between fcc and bcc structures [25]. We never detected Ni_3Al as intermediate phase.

4. Discussion

4.1. Accommodation of the non-stoichiometry in NiAl

The NiAl phase is centred around the composition 50 at % Ni. It consists essentially of ordered body cubic centred alloys having B2 type crystallographic structure like CsCl (Table I). The (0 0 0) sites and the $(\frac{1}{2}\frac{1}{2}\frac{1}{2})$ sites are, respectively, occupied by Ni and Al atoms. In the $\langle 1\,1\,1 \rangle$ directions, the (1 1 1) planes are alternately filled with Al and Ni atoms (Fig. 12).

At stoichiometric composition, the compound NiAl has a long-range order degree of 1 up to 1000° C, a degree which remains close to 1 at higher temperatures, below the melting point [26].

The NiAl phase can accommodate large deviations from the stoichiometry as reported in Fig. 1, from 58 to 31 at % Al. On the Al-rich side, the deviation from stoichiometric composition is accommodated by vacancies on the lattice of Ni atoms ($Ni_{1-x}\square_x Al$). Depending on heat treatment and composition, some workers show that the vacancies may be ordered [21, 27]. At the Ni_2Al_3 composition (Al = 60 at %), one-third of the Ni sites are vacant and a rearrangement of the vacancies occurs. Every third (1 1 1) Ni plane perpendicular to the cube diagonal $\langle 1\,1\,1 \rangle$ of the primitive cell is absent. The ordering reduces the crystal symmetry from cubic to hexagonal. The cell of Ni_2Al_3 is related with the NiAl cubic cell

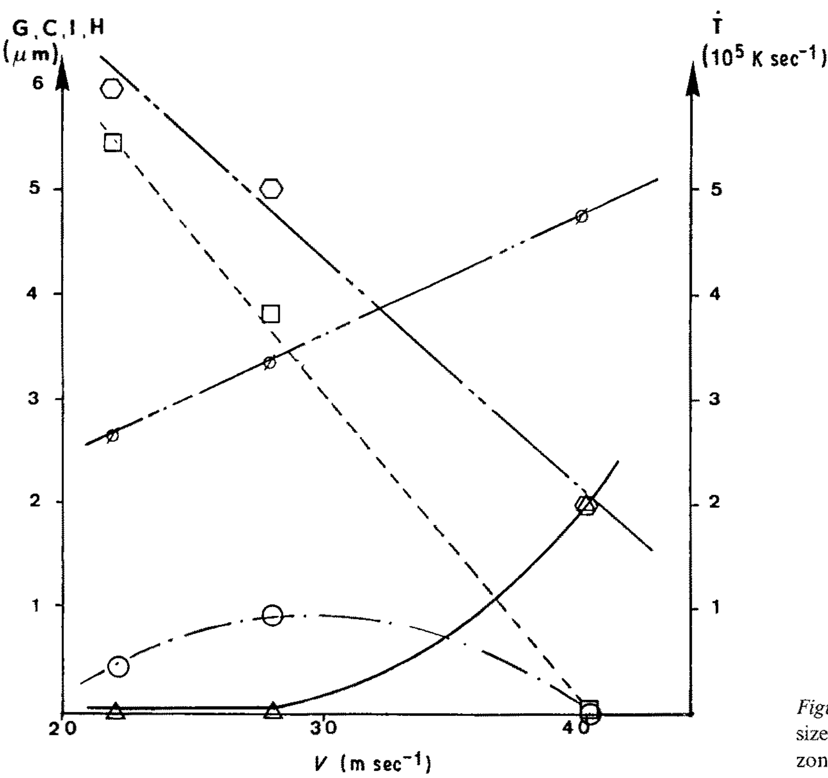

Figure 11 Influence of the rolling velocity on the size of (⬡) the grain, (○) core, (△) intermediate zone and (□) petals.

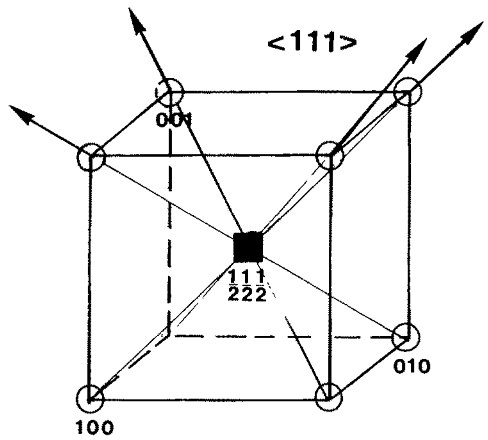

Figure 12 Ni–Al cell and ⟨1 1 1⟩ directions showing the formation of Ni_2Al_3 axial domains. (■) Al, (○) Ni.

with:

$$\boldsymbol{a} \parallel \langle 1\,1\,0\rangle \text{ NiAl} \quad a = a_0\sqrt{2}$$

$$\boldsymbol{c} \parallel \langle 1\,1\,1\rangle \text{ NiAl} \quad c = a_0\sqrt{3}$$

where a_0 is the lattice parameter of the NiAl primitive cell. Owing to the missing planes, there is a small collapse ($c/a = 1.214$) along the $\boldsymbol{c}$ axis (theoretical $c/a = 1.225$).

4.2. Changes of composition during cooling

The solidification of microcrystallized alloys, is carried out with different steps according to the peritectic reaction occurring at 1133° C, in the binary NiAl system

$$\text{NiAl (bcc)} + \text{liq} \rightleftharpoons Ni_2Al_3 \text{ (h)}$$

As the temperature decreases, the first crystal formed from the liquid is the NiAl (bcc) phase. During slow cooling rate, the undercooling ΔT is small, the inner part (C) of the grain is formed at high temperature ($T = 1560°$ C) and the first NiAl (bcc) crystallites have a near stoichiometric composition

$$Ni_{46.5}Al_{53.5} = Ni_{0.87}\square_{0.13}Al$$

This phase forms the centre of the grains, and retains all the characteristics of the near stoichiometric compound with a network of dislocations due to stresses occurring during quenching.

During slow cooling, the composition of the NiAl phase changes according to Fig. 1, until it reaches a composition near $x = 0.33$ ($Ni_{0.66}\square_{0.33}Al$) where the cubic structure of NiAl becomes unstable and transforms peritectically into Ni_2Al_3

$$Ni_{0.66}\square_{0.33}Al \text{ (bcc)} + \text{liq} = Ni_2Al_3 \text{ (h)}$$

The orientation of Ni_2Al_3 crystallites (region I) formed with this reaction is directly related to the crystallographic orientation of the NiAl primitive phase, as previously mentioned. Four types of Ni_2Al_3 axial domains corresponding to the four possible (1 1 1) planes of NiAl may coexist (Fig. 12). On cooling, the Ni_2Al_3 axial domains are formed by nucleation and grow from the NiAl primitive cell. The axial domains have a small size (< 50 nm).

At slow cooling rates, well-oriented Ni_2Al_3 crystals may grow according to the thermal gradient in the ribbon. The region (H) is formed of large domains of Ni_2Al_3 oriented with ⟨0 0 0 1⟩ or ⟨1 1 2 1⟩ directions parallel to the thermal gradient. The orientation of the domains in this region is directly related to the thermal gradient existing in the ribbon during solidification.

4.3. Influence of cooling rate on the structure of a dendrite grain

The respective size of the different regions (C, I, H, E) depends on the cooling rate. The mean size of the grains in the case of Cr-doped alloys decreases from 6 to 2 μm for a cooling rate increasing from 2.6×10^5 to 4.7×10^5 K sec^{-1}.

The undercooling, ΔT, increases with the cooling rate, and for high cooling rate, the solidification begins at low temperature. For $V = 40$ m sec^{-1}, the undercooling ΔT ($\dot{T} = 4.7 \times 10^5$) is sufficient to promote the solidification of the $Ni_{1-x}\square_xAl$ phase in the composition range of the peritectic reaction ($x = 0.33$). In the case of Cr-doped alloys, for high cooling rates, the core (C) is very small and often is not detected even by TEM. Moreover, as the undercooling is high, the number of nucleation centres is also high and the intermediate zone (I) is very large, but the Ni_2Al_3 (h) crystallites cannot grow. The size of zone H remains small as represented in Fig. 8b.

The results described here are in good agreement with observations of some authors. As shown by Fehling and Scheil [28] and Kattamis and Flemmings [29], the microstructure is directly related to the undercooling ΔT. For small values, these authors obtain a typical dendritic structure. With increasing undercooling, the microstructure changes with star-like dendrites. At greater undercooling level, the microstructure becomes more spherical. The change in the morphology is abrupt at a certain degree of undercooling typical of the alloy. In the case of Cr-doped alloy, a change in the grain morphology around $V = 35$ m sec^{-1} ($\dot{T} = 4.10^5$ K sec^{-1}) was effectively found.

4.4. Influence of the dopant on the shape of the grain

Microcrystallized ribbons of Cu-, Fe- or Ti-doped alloys also exhibit dendritic grains. These grains show the same complex structure with four zones but the respective size of the different regions is directly related to the nature of the dopant. With Cr additions, the NiAl core remains large. According to Fasman and Raiskina [30], NiAl phase is stabilized by Cr and the extension of the NiAl core is important.

In the case of Fe or Cu additions, the solidifcation behaviour of the alloys is very similar to the undoped alloy due to the large solubility of these elements in Ni_2Al_3.

4.5. Texture of an Ni crystallite

The Al removal from the Cr-microcrystallized alloys begins in the external zone (E) and occurs progressively to the core of the structure. The attack of the Ni_2Al_3 petals (H) and of the intermediate zone (I) gives rise to the Ni fcc, which is well oriented with the NiAl primitive cell, with intermediate zones of NiAl and Ni_2Al.

Because of the Al-removal from the Ni_2Al_3 phase, intermediate NiAl crystallites first appear with typical orientation relationship with the primitive Ni_2Al_3 phase. Then the Ni crystallites are formed by attack of these crystallites.

Aluminium leaching is not random; it shows a step by step evolution which can be summarized by the scheme

$$Ni_2Al_3\ (h) \Rightarrow NiAl\ (cc) \Rightarrow Ni_2Al\ (h) \Rightarrow (fcc)$$

and will be developed in other work [31].

5. Conclusion

The metallurgical study allows us to master the structural states of the starting alloy, and the homogenized and microcrystallized alloys. The starting alloy presents different phases. On annealing at high temperatures, we obtained a homogeneous alloy in the case of Fe or Cu dopant. The melt-spinning allows control of the growth of the NiAl and Ni_2Al_3 phases according to the peritectic reaction: $NiAl + liq \rightleftharpoons Ni_2Al_3$. From these three alloys, three catalysts have been prepared. In every precursor Cr-doped alloy, the chromium appears as a texture-promoting factor and a surface stabilizer. The homogeneity of the alloy and its crystallization state have a very important effect on the residual amount of aluminium and on the superficial chromium.

Acknowledgements

This study was supported by the CNRS (Chemical ATP no. 904332) and was conducted in a Stimulation Plane of the CEE (CODEST program). One author (J. G.) thanks IMPHY SA (France) for a research grant.

References

1. M. HANSEN and A. ANDERKO, "Constitution of binary alloys" (McGraw-Hill, New York, 1958).
2. J. FREEL, W. J. M. PICKER and R. P. ANDERSON, *J. Catalysis* **16** (1970) 281.
3. A. J. BRADLEY and A. TAYLOR, *Phil. Mag.* **23** (1937) 1049.
4. C. J. SMITHELLS, "Metals Reference Book" (Butterworths, London, 1955).
5. A. B. FASMAN, S. D. MIKHAILENKO, N. A. MAKSIMOVA, Zh. A. IKHSANOV, V. Y. KITAIGORODSKAYA and L. V. PAVLYKEVITCH, *Appl. Catalysis* **6** (1983) 1.
6. C. KORDULIS, B. DOUMAIN, J. P. DAMON, J. MASSON, J. L. DALLONS and F. DELANNAY, *Bull. Soc. Chim. Belg.* **94** (1985) 371.
7. B. IMELIK, G. A. MARTIN and A. J. RENOUPREZ, "Catalyse par les métaux" (CNRS, Paris, 1984).
8. L. KAUFMAN and H. NESOR, *Met. Trans.* **5** (1974) 1623.
9. P. G. NASH, V. VEGINS and W. W. LIANG, *Bull. Alloys Phase Diagrams* **3** (1982) 367.
10. M. KHAIDAR, Thesis, Institut National Polytechnique de Grenoble (1981).
11. P. CASANOVA, J. C. JOUD, C. SENILLOU and A. R. YAVARI, *Mem. Sci. Revue Met. Fr.* **81** (1984) 553.
12. R. S. CARBONARA, R. V. RAMAN and A. J. CLAUER, Proceedings of the 4th International Conference on Rapidly Quenched Metals, edited by T. Masumoto and K. Suziki, Sendai (Japan Institute of Metals, 1981) p. 15.
13. P. FOURNIER and M. HENRY, *Rev. Gen. Elec* **92** (1983) 314.
14. "Microanalyse, Microscopie Electronique à Balayage", Ecole d'Eté, Saint Martin d'Hères, (CNRS, Paris, 1978).
15. K. EMMERICH, in "Rapidly Quenched Metals", edited by S. Steeb and Warlimont, (Elsevier, Amsterdam, 1985) p. 71.
16. M. BLANK, C. CAESAR and U. KÜSTER, *ibid.*, p. 883.
17. D. SZEWIECZEK, J. TYRLIK-HELD and A. WASZCZUK, *ibid.*, p. 1791.
18. F. FAYARD, F. DUFLOS and A. LASALMONIE, *ibid.*, p. 811.
19. M. HILLMAN and H. R. HILZINGER, "Rapidly Quenched Metals", Vol. 1, (London, 1978) p. 22 (cited by P. Fournier and M. Henry [13]).
20. E. P. LAUTENSCHLAGER, T. C. TISONE and J. O. BRITTAIN, *Phys. Status Solidi* **20** (1967) 443.
21. R. De RIDDER, G. VAN TENDERLOO and S. AMELINCKX, *ibid.* (*a*) **43** (1977) 133.
22. F. REYNAULT, *J. Appl. Crystallogr.* **9** (1976) 263.
23. F. DELANNAY, *Reactiv. Solids* **2** (1986) 235.
24. V. BIRKENSTOCK, R. HOLM, B. REINFANDT and S. STROP, *J. Catalysis* **93** (1985) 55.
25. C. M. WAYMAN, "Physical Metallurgy", Part II, edited by R. W. Cahn and P. Haasen (North Holland Physics, Amsterdam, 1985).
26. T. HUGHES, E. P. LAUTENSCHLAGER, J. B. COHEN and J. O. BRITTAIN, *J. Appl. Phys.* **42** (1971) 3705.
27. P. DELAVIGNETTE, H. RICHEL and S. AMELINCKX, *Phys. Status Solidi* (*a*) **13** (1972) 545.
28. J. FEHLING and E. SCHEIL, *Z. Metallkde* **53** (1962) 593.
29. T. Z. KATTAMIS and M. C. FLEMMINGS, *Trans. AIME* **236** (1966) 1523.
30. A. B. FASMAN and F. I. RAISKINA, *Russ. J. Phys. Chem.* **50** (1976) 1037.
31. J. GROS, S. HAMAR-THIBAULT and J. C. JOUD, *Surface and Interface* **11** (1988) 611.

Received 21 October 1987
and accepted 17 February 1988